

Liquid-crystal-droplet optical microcavities

Matjaž Humar

To cite this article: Matjaž Humar (2016) Liquid-crystal-droplet optical microcavities, Liquid Crystals, 43:13-15, 1937-1950, DOI: [10.1080/02678292.2016.1221151](https://doi.org/10.1080/02678292.2016.1221151)

To link to this article: <http://dx.doi.org/10.1080/02678292.2016.1221151>



Published online: 15 Aug 2016.



Submit your article to this journal [↗](#)



Article views: 119



View related articles [↗](#)



View Crossmark data [↗](#)

INVITED ARTICLE

Liquid-crystal-droplet optical microcavities

Matjaž Humar ^{a,b}

^aCondensed Matter Department, J. Stefan Institute, Ljubljana, Slovenia; ^bHarvard Medical School and Wellman Center for Photomedicine, Massachusetts General Hospital, Cambridge, MA, USA

ABSTRACT

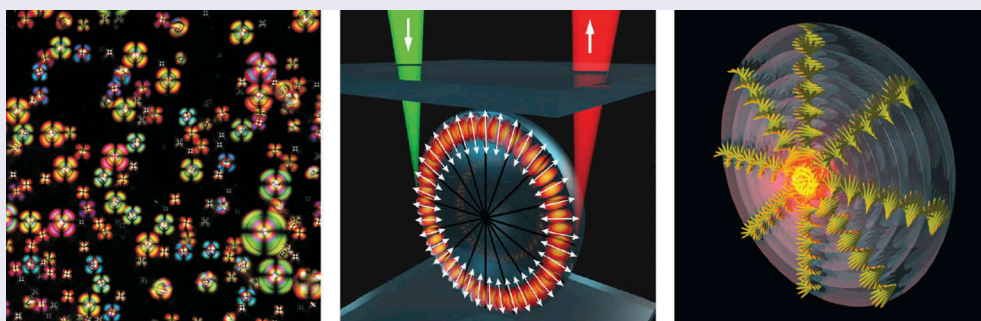
The use of liquid-crystal droplets as optical microcavities and lasers is reviewed and possible applications are discussed. Liquid-crystal droplets are prepared by simple methods that enable scalable production since their internal structure is formed by self-assembly. Light is trapped in droplets due to total internal reflection on the surface due to refractive index mismatch or because of a photonic bandgap structure in cholesteric liquid crystals (CLCs). Light confinement gives rise to a variety of optical modes and by employing a fluorescent dye and external optical pumping, lasing can be achieved. Liquid-crystal-droplet cavities are largely tunable by applying an electric field or a temperature change. Such cavities can be used as temperature and chemical sensors, and tunable light sources and filters in future integrated soft photonic circuits.

ARTICLE HISTORY

Received 1 May 2016

KEYWORDS

Liquid-crystal droplets; optical cavities; lasers; whispering-gallery modes; cholesteric lasers



1. Introduction

In recent years, there has been great advancement in manufacture of micro-optical components and integrated optic circuits made of solid-state materials. These components are traditionally manufactured by top-down procedures such as lithography. Alternatively, liquid crystals (LCs) could provide simpler manufacturing process of these components by the use of self-assembly of very complex structures [1–5] and provide large tunability [6,7]. LCs are used for a wide variety of optical applications ranging from liquid crystal displays (LCDs) to cholesteric liquid crystal (CLCs) lasers [8]. Traditionally, however, these devices are large in size, typically the LC is confined in one dimension to micrometre scale and extended in the other two dimensions up to meter scale. In order to produce microoptical components, we need to confine LCs to very small size. The easiest way is to make microdroplets embedded in a liquid or solid matrix which gives a particular surface anchoring. An example of such

system are the polymer dispersed liquid crystals (PDLCs) [9,10], which are mainly used for switchable windows. The size of the droplets is usually in the order of few micrometers, so that the scattering of light is as high as possible. PDLCs can also be used for active optical components such as random lasers [11–13]. In PDLCs, usually collective optical properties of many droplets combined is used, so single droplets are not regarded as optical cavities. In order to use LC droplets as cavities, they have to be larger than approximately 10 μm . Methods for preparation of PDLCs such as phase separation give too small droplets and they are usually of irregular shapes and densely packed which limits the use of single droplets. In order to use liquid crystal as optical cavities, single droplets have to be generated, manipulated and studied. There are many studies of generation and study of liquid crystal droplets and shells, and of the complex configurations formed within [14,15]. Here an overview of optical cavities in LC droplets is overviewed and further directions are discussed.

2. Whispering-gallery mode cavities

Whispering-gallery mode (WGM) cavities are made of a circular or spherical transparent object such as disc, sphere or toroid. Here we will only consider spheres. If the refractive index of the object is greater than the index of the outside medium, the light can be trapped inside the sphere as a consequence of multiple total internal reflections and circulates close to the surface. After one circulation, if the light comes to the same point in phase, the resonant condition is met. In general, WGMs are solutions of Maxwell's equations in spherical coordinates for a dielectric sphere. The wavelengths of the resonances are uniquely characterised by a set of three mode numbers, the radial mode number q , the polar mode number l , the azimuthal mode number m and the polarisation p . The radial mode number indicates the number of maxima in the radial intensity distribution in the sphere, the polar mode number gives the number of wavelengths for one circulation of the light and the azimuthal mode number indicates the inclination of the circular orbit. In sphere with uniform distribution of refractive index, all the planes in which the light circulates are equivalent, so the modes are degenerate in regard to azimuthal mode number m . However, as soon as the spherical symmetry is broken by either deformation of the sphere or non-uniform refractive index distribution, modes with a particular q and l are split into modes with different m . For large spheres ($l \gg 1$) and $q = 1$, the approximate solutions are given by

$$2\pi r n_1 \approx l\lambda, \quad (1)$$

where r is the radius of the sphere, n_1 is the refractive index of the sphere and λ is the wavelength of the mode. Better solutions can be calculated using precise analytical approximations [16] and exact solutions can be calculated numerically by using spherical Bessel and spherical Hankel functions [17].

WGMs are well known for their very high Q-factors combined with small size. For large spheres and $q = 1$ the Q-factor due to radiative leaking of light caused by the curvature can be approximated as

$$Q = \frac{\lambda}{\Delta\lambda} \approx e^{8r/\lambda(n_1-n_2)^{3/2}}, \quad (2)$$

where $\Delta\lambda$ is the linewidth of the resonance and n_2 is the refractive index of the surrounding media. The Q-factor is exponentially dependent on the microcavity size compared to the wavelength as well as the refractive index contrast between the inside and outside of the sphere. Absorption and scattering in the material as well as surface roughness can substantially reduce the Q-factor. LCs

are usually transparent to visible light, so that the absorption does not contribute much. The surface of a droplet created by surface tension is also typically very smooth. The largest contribution to the decreased Q-factor may be contributed to light scattering on thermal fluctuations of the local director orientation [18].

The WGMs can be in general observed and measured in two ways. The first one is by coupling the cavity through an evanescent field to an optical waveguide, for example, a tapered fibre or prism [19,20]. When the wavelength of the external light matches to one of the optical modes in the cavity, the light is coupled out of the waveguide and reduces its transmission. This method requires the optical waveguide to be positioned closer to the cavity than the wavelength of the light. The second method to observe WGMs is to dope the cavity material with a fluorescent dye and excite it with an external laser. Due to the Purcell effect [19], the spontaneous emission from the dye is enhanced at wavelengths corresponding to the optical modes. Therefore, in the emission spectrum from a WGM cavity, characteristic spectral lines appear. By using a pulsed excitation laser, the dye-doped WGM cavities can also be operated in lasing regime. Using a nanosecond pump laser and cavity with several mM concentration of an organic dye, the minimum required cavity Q-factor to achieve lasing [21] is approximately 10^4 . For a sphere with $n_1 = 1.7$ in water environment $n_2 = 1.33$, the minimum size of the cavity to achieve lasing calculated using (2) is $\sim 10 \mu\text{m}$.

2.1. WGMs in nematic droplets

WGMs were studied in nematic droplets with homeotropic anchoring, which is the simplest geometry for LC droplets. In this case, the director configuration is radial, meaning that the director is pointing in the radial direction in every point of the droplet and forms a radial hedgehog defect at the centre of the droplet, visible as a dark spot (Figure 1(a)). When observed under crosses polarisers, a typical cross is observed (Figure 1(b)). The droplets were made by mechanical mixing of a small quantity ($\sim 1\%$) of nematic liquid crystal E12 with PDMS polymer, which was left to polymerise at room temperature, making a solid matrix for stabilising the droplets. Alternatively, the droplets were dispersed in water containing 4 mM of sodium dodecyl sulfate (SDS) to achieve homeotropic anchoring. The droplets made by this method are polydispersed, with sizes ranging from $1 \mu\text{m}$ to $50 \mu\text{m}$ (Figure 1(c)). Because of surface tension, they have almost perfect spherical shape and smooth surface. Before mixing with PDMS or water,

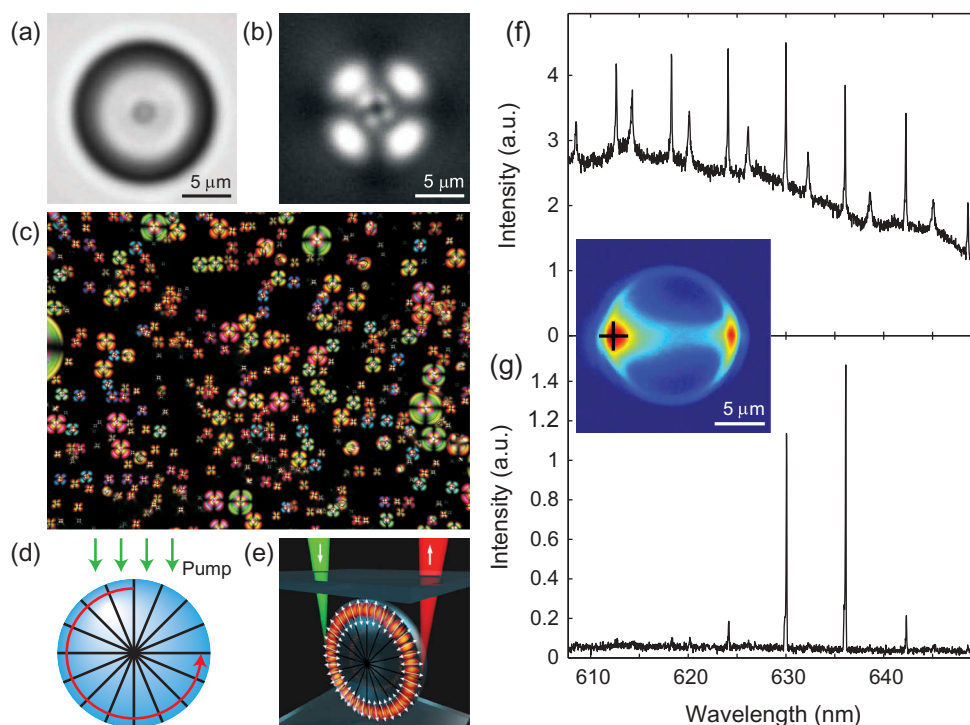


Figure 1. (Colour online) (a) Bright-field image of a radial nematic droplet and (b) the same droplet under crossed polarisers. (c) Colour image of dispersion of nematic droplets under crossed polarisers. (d) Principle of WGMs in nematic droplets and (e) 3D rendering of light excitation and circulation. (f) Spectrum of light from a droplet below lasing threshold and (g) above lasing threshold (inset). False colour image representing the fluorescent intensity of a droplet illuminated by a laser at the position of the cross.

the LC was doped with 0.1 wt% fluorescent dye. In general, almost any fluorescent dye soluble in LC can be used. When a droplet is illuminated with a laser matched with the absorption of the dye, part of the light is coupled to the WGM circulating in the droplet (Figure 1(d)). A single droplet was illuminated by a focused 532 nm laser beam near its edge (Figure 1(e)). A bright spot of fluorescent light was observed at the point of the laser beam as well as on the opposite side of the droplet corresponding to the circulating light (inset of Figure 1(f)). In the spectrum of the light emitted by a single droplet, sharp spectral lines can be observed (Figure 1(f)). Since the droplet is birefringent, transverse-electric (TE) and transverse-magnetic (TM) light polarisations experience different refractive indices. In isotropic sphere, the two polarisations have almost the same wavelength, however, here we need to write two separate Equations (1). The TE polarisation has the electric field parallel to the surface of the droplet, therefore, it is perpendicular to the nematic director and experiences ordinary refractive index, while TM polarisation is perpendicular to the droplet surface, so along the director and experiences extraordinary refractive index. For ($q = 1$), we have $2\pi n_o \approx l_{TE}\lambda_{TE}$ and $2\pi n_e \approx l_{TM}\lambda_{TM}$. By calculating exact solutions of the modes in a nematic droplet, we

see that the TE sees only ordinary refractive index, whereas TM modes couple both ordinary and extraordinary indices [22]. In Figure 1(f) two sets of modes are visible. The modes with sharper spectral lines are first radial TM modes ($q = 1$) and the ones with broader lines are second radial TM modes ($q = 2$). TE modes are not observed, since they have too low refractive index contrast and therefore too low Q-factor.

When the dye-doped droplets are pumped with a pulsed laser above certain energy threshold, lasing can be achieved [23]. Only WGM which have high enough Q-factor and are in the wavelength region where the dye has the highest gain, start to lase (Figure 1(g)). In this case only few first radial TM modes are lasing. Their intensity is much higher than the fluorescent background.

2.2. Electric tuning of the modes

One of the greatest advantages of LCs to make optical components in comparison with the solid-state counterparts is the large tunability, especially with electric field, which simplifies integration with existing electric circuits. Also, solid-state optical cavities can be tuned by using electro-optic effect, albeit to a much less amount. For example, a lithium niobate microring

resonator was tuned by 0.006% by applying electric field of $1.5 \text{ V}/\mu\text{m}$ [24]. Another way of tuning the modes is to embed a solid state-resonator in a LC material. The tuning only affects the evanescent field, which represents only a small fraction of the total electric field of the WGMs, making the tunability much lower than when having the liquid crystal inside the cavity [22,25]. For example, a tunability of 0.01% was achieved when applying $2 \text{ V}/\mu\text{m}$ [26].

The electric field effect in radial nematic droplets have been studied before [27]. As the field is applied, the molecules of the positive dielectric anisotropy LC start to rotate in the direction of the field. There is almost no distortion very near the surface because of the strong anchoring and radial hedgehog point defect is still present in the centre (Figure 2(a)). The transition from completely radial configuration to this distorted configuration is continuous and without hysteresis, therefore, this range is used for the tuning of the WGMs. When higher field is applied, the structure of the droplet is transformed into a $+1/2$ defect ring circulating the droplet at the surface and an almost uniform director configuration in the centre (Figure 2(a)). This transition happens at certain voltage threshold and it is discontinuous and has a hysteresis when the field is reduced. In the experiments, a $16 \mu\text{m}$ droplet was subjected to a continuously increasing alternating electric field up to $2.1 \text{ V}/\mu\text{m}$ at 50 kHz and WGM spectra were recorded (Figure 2(c)). The same as in Figure 1(f), first and second radial TM modes are visible. First radial modes are visible as thinner lines due to higher Q-factor, while second radial modes are visible as thicker lines. At zero field, the modes experience the extraordinary refractive index, but when the

electric field is applied, the molecules rotate and the modes experience lower refractive index. This decreases the optical path length and the modes undergo a blue shift. This is the case for both first and second radial modes. The first radial modes, however, experience smaller shift, since they are located closer to the surface of the droplet where the distortion of the director is smaller because of strong surface anchoring. The tunability is also dependent on the size of the droplets, since in smaller droplets, the effect of the anchoring is more important, meaning that the tunability is lower. Tunability as high as 20 nm (3%) in $17 \mu\text{m}$ diameter droplet at $2.6 \text{ V}/\mu\text{m}$ was achieved. This is one to two orders of magnitude larger compared to other types of electrical tuning [24,26,28,29].

2.3. WGMs in other LC droplets

In principle, WGMs can be achieved in droplets made out of almost any LC, including smectic, ferroelectric, cholesteric, discotic and more exotic phases. The most important condition is that the refractive index of the LC should be larger than the surroundings. Further, the LC should be transparent and does not contain too many defects, which scatter light. For example, ferroelectric liquid crystals (SmC^*) are known for their fast switching under applied electric field and could be a good candidate as a material for droplets used for WGM microcavities instead of nematic LCs. We have achieved lasing in a droplet of Nile red-doped ferroelectric liquid crystal (Kingston Chemicals) in PDMS (Figure 3). The produced droplets are, however, not completely spherical and their internal structure is also in most cases full of defect lines. Because of non-spherical shape, each lasing line is split in

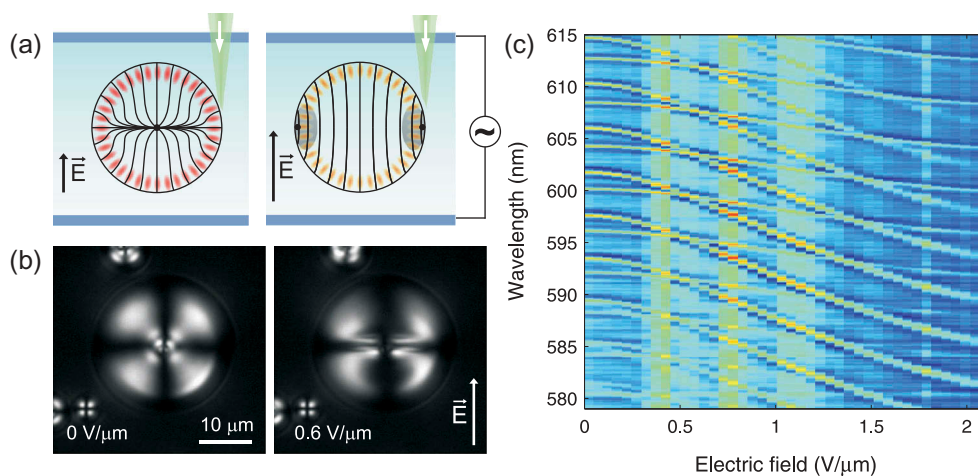


Figure 2. (Colour online) (a) Nematic director at small and large electric field in relation to the circulating WGMs. (b) A nematic droplet at zero and $0.6 \text{ V}/\mu\text{m}$ applied in plane imaged under crossed polarisers. (c) Spectrum of WGM from a single droplet when the electric field is increased up to $2.1 \text{ V}/\mu\text{m}$.

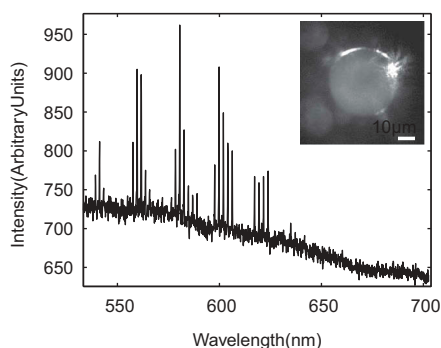


Figure 3. Lasing spectrum from a SmC* droplet (inset) image of laser light emitted by the droplet.

more lines with different azimuthal mode number m . WGMs have been observed by other groups in SmA droplets [30] and tubes [31].

2.4. Temperature tuning of the modes

Another way of tuning WGMs is by changing the temperature [32], which changes the refractive index and size of the cavity. For solid state-materials, the temperature tunability is quite small, in the order of 10–300 pm/K [33,34]. However, for LCs the refractive index is highly temperature dependent and enables large tunability. WGMs in a 24 μm diameter E12 droplet in SDS solution in water was studied as temperature was increased from room temperature to above the clearing point of the LC. In the spectrum of the light emitted for a droplet, several distinct spectral lines are observed, which shift at different rates and in different directions (Figure 4). There are four sets of TM modes with radial mode numbers 1–4 and two sets of TE modes with radial mode numbers 1 and 2. The TM modes shift to shorter wavelengths, while the TE modes shift to longer wavelengths (Figure 4(a)). The TM polarisation is associated with extraordinary refractive index, which decreases with temperature; and the TE polarisation is associated with ordinary refractive index, which on the other hand increases with temperature. The experimental results agree well with calculation of the modes [16] taking into account LC refractive index change with temperature (Figure 4(b)). The shift in TM WGMs is approximately 15 nm for the temperature change from 25°C to 55°C.

When the temperature is approaching the nematic to isotropic transition (59°C), the modes begin to shift in a more chaotic way, since the director configuration is changing and the LC is partially melting. Above $\sim 59^\circ\text{C}$, the transition into isotropic phase is complete and both TE and TM modes have the same refractive index and are visible as mode pairs. With further increasing temperature,

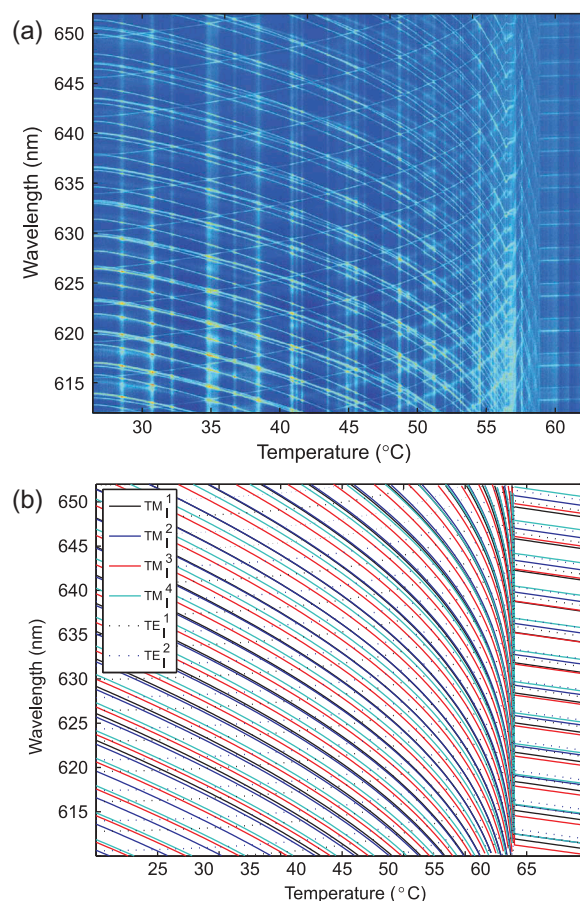


Figure 4. (a) Spectrum of light emitted by a nematic droplet as a function of temperature. (b) Calculated positions of WGMs when taking into account temperature dependence of the refractive index of the LC.

the modes do not experience any large shift any more, since the isotropic liquid does not have large temperature dependence of the refractive index.

Instead of changing the temperature of the whole sample, individual droplets were heated by using a focused infrared laser beam at 1064 nm. The tuning of the WGMs up to 6 nm was achieved when illuminating a droplet with 140 mW of optical power.

Due to their high Q-factors, solid WGM cavities are used as very precise temperature sensors [33,34]. LCs have very large dependence of refractive index upon temperature, therefore, they are even more suited to the measurement of the temperature. On the other hand, this is also a disadvantage, since LC microoptical components need good temperature control for their stable operation. WGMs in LC droplets can also be used to study LC phase transitions and surface anchoring. Both can considerably change optical properties and alter the wavelength or Q-factors of WGM. For example, smectic-A (SmA) to nematic phase transition was studied by measuring the quality factor in droplets of 8CB [30].

2.5. Chemical sensing

Both WGMs and LC droplets have been separately extensively studied for chemical sensing. WGM frequencies are sensitive to the refractive index change near the surface of the cavity. Therefore, the change on either side of the surface, such as molecules binding, can be detected. Due to extremely high Q-factors, the WGM cavities are incredibly sensitive and can detect minute amounts of analytes, single viruses and down to single molecules [35,36].

LCs in the form of thin layers with one surface in contact with water have been also used as sensitive sensors [37]. The surface anchoring can be changed by absorption of molecules to the surface. Because of long range interactions in LCs, the anchoring also affects the bulk liquid crystal, so the changes can be easily observed under a polarising microscope. Changes in surface anchoring can be also be studied in LC droplets. The structural transitions in droplets [38] have been used for detection of various analytes, including extremely small concentrations of endotoxins [39], proteins [40], bacteria and viruses [41] and identification of cancerous cells [42]. The advantage of droplets is, that they do not need any mechanical support or surface treatment, they are small and can be introduced into a microfluidic chip. In most of the LC chemical sensors, the structural transitions are observed under an optical/polarisation microscope, which does not enable detection of small changes in anchoring. Therefore, it is beneficial to measure the orientational changes in LCs by employing WGMs.

In our demonstration, we have used Nile red fluorescent dye-doped droplets of a nematic LC 5CB dispersed in water. A single droplet was pumped by a pulsed green laser (532 nm) to achieve lasing and at the same time, held in place in a microfluidic channel by using an infrared optical tweezers (1064 nm). Water containing different concentrations of SDS surfactant was flown through the microfluidic channel and the lasing spectra was observed in real time. When the SDS concentration was increased from 0 to 2 mM, the anchoring changed from planar to homeotropic and the droplet experienced a continuous transition from a bipolar to a radial configuration (Figure 5(a)). The lasing spectrum also changed starting at 0.2 mM and after 0.6 mM remained constant (Figure 5(b)). In pure water, when the droplets are in a dipolar configuration, the spherical symmetry in the droplet is broken, therefore, the different azimuthal modes are not degenerate and the lasing spectrum contains four lasing peaks split into a number of subpeaks with a separation of 0.5 nm (Figure 5(c)). At concentrations higher than 6 mM, the

director configuration near the surface, where the WGMs are located, is almost radial, so the lasing spectra (Figure 5(d)) is identical to the one in radial configuration (Figure 1(g)).

The major advantage in using the laser emission to determine droplet configuration is simplified and faster readout. There is no need of imaging, which is slow, requires an optical microscope and image analysis. On the contrary, spectral fingerprint can be measured in fast moving droplets, for example, in a microfluidic channel. The pumping and detection can be carried out through a single optical fibre. Further, instead of only identifying if the droplet is in bipolar or radial configurations, intermediate states can be identified, so smaller structural changes and therefore concentrations can be detected. For our example, the WGMs start to change at already 0.2 mM, while the radial structure is formed only above 1 mM.

3. Bragg cavities

A one-dimensional (1D) periodic structure or 1D photonic crystal, also known as Bragg reflector, has a photonic bandgap and reflects light in a wavelength region corresponding to its periodicity. Bragg reflectors are widely used as mirrors, distributed Bragg reflector lasers, filters, etc. A convenient way to make a Bragg reflector or a laser is employing LCs, including a variety of liquid crystal phases such as cholesteric phase, chiral smectic phase, cholesteric elastomers and polymers and blue phases [8,43]. The periodic structure is formed spontaneously and can be tuned. By adding a fluorescent dye as gain material and applying external optical pumping, lasing can be achieved. Lasing occurs at the short or long wavelength edge of the photonic bandgap. However, if a thin defect layer is embedded into the LC, then the lasing occurs inside the photonic bandgap. The photonic bandgap exists in between $\lambda_1 = n_o p$ and $\lambda_2 = n_e p$, where p is the helical pitch length.

2D and 3D photonic crystals confine light also in the other dimensions. These structures are, for example, made of periodic holes in a thin substrate or regular assemblies of small spherical particles know as opals. Colloidal assemblies in LC are also attractive candidates for photonic crystals [1,7]. 3D photonic crystals have a photonic bandgap that is direction dependent and if the refractive index contrast of the structure is not high enough, there is no complete bandgap [44]. Lasing has been achieved in a 3D photonic crystal [45], however, the assembly of such lasers is extremely complicated and time consuming. Lasing in a 3D photonic

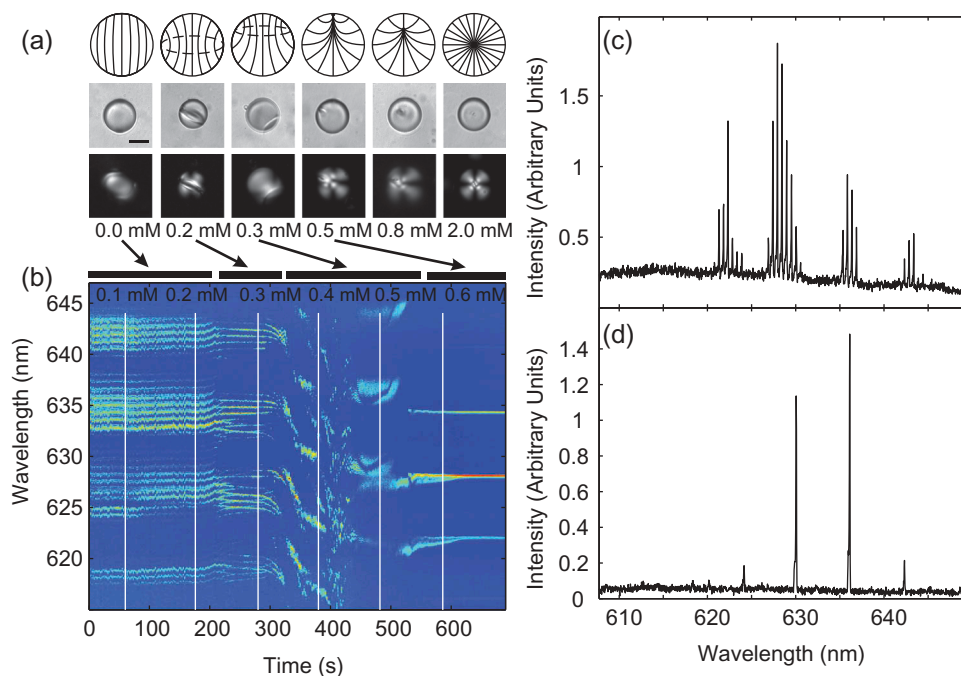


Figure 5. (Colour online) (a) Nematic director configurations (top), bright-field microscope images (middle) and crossed polarisers images (bottom) of droplets when subject to increasing concentration of SDS surfactant. (b) Spectrum of lasing of WGMs in time of a single droplet in a microfluidic channel when solutions of increasing concentrations of SDS are added. (c) Lasing spectrum in pure water and (d) in high concentration of SDS.

crystal has been also achieved in a blue phase [46], with the lasing with different wavelengths being emitted in three orthogonal directions.

Another way of making a 2D or 3D photonic bandgap structure is to use concentric rings for a planar structure or concentric shells for a spherical onion structure. This structures are basically composed of a 1D photonic reflector wrapped around the central point. Light going out from this central point is reflected back by the periodic structure and is confined in the centre. A number of 2D circular Bragg structures have been realised in 2D using standard lithography and lasing has been demonstrated [47]. However, 3D onion Bragg cavities are difficult to manufacture [48,49] and lasing has not been achieved in these solid-state structures.

3.1. CLC droplet omnidirectional laser

CLC droplets with planar anchoring are a natural candidate for a Bragg onion cavity [50]. Their spherulite structure has been studied already many years ago [9,51]. Recent simulations show the detailed structure of cholesteric droplets [52] and existence of a rich zoo of free standing topological knots [15]. To observe the structure of CLC droplets, a mixture of a nematic liquid crystal and chiral dopant was mixed to produce a 2.2 μm pitch. This mixture was dispersed in glycerol by mechanical mixing. The periodic structure in the radial direction

is clearly visible (Figure 6(a and b)), as well there is a double helix [52] visible as a dark line extending from the centre to the surface of the droplet. To make a laser, MLC-7023 liquid crystal was mixed with 25.5 wt% S-811 chiral dopant and 0.2 wt% fluorescent dye Nile red. This mixture is similar to the ones used for planar CLC lasers [8]. The droplet was uniformly illuminated through a 20 \times objective with a 532 nm Q-switched laser with repetition rate of 200 Hz. The laser light was generated along the axis of the helical twist and was therefore propagating out of the droplet in all directions (Figure 6(c and d)). The laser emission was visible as a bright spot in the centre of the droplet (Figure 6(e)). In the spectrum of the emitted light, there was a single laser line, with linewidth of 0.1 nm, located at long wavelength edge of the photonics bandgap, indicating band-edge lasing (Figure 6(e)). The lasing wavelength is only very slightly dependent on the droplet size. Threshold behaviour in the pump output curve further confirms lasing was indeed observed. The lasing threshold of a 40 μm diameter droplet is 1.7 mJ/cm^2 or 20 nJ. The highest achieved output power of a single droplet is 0.05 mW. The smallest droplets still lasing had a diameter of 15 μm . This size could be further decreased by using higher birefringence LC, using higher concentration of the fluorescent dye and shorter lasing wavelength. The polarisation of the output laser light was circular. Lasing wavelength, threshold energy density, linewidth and

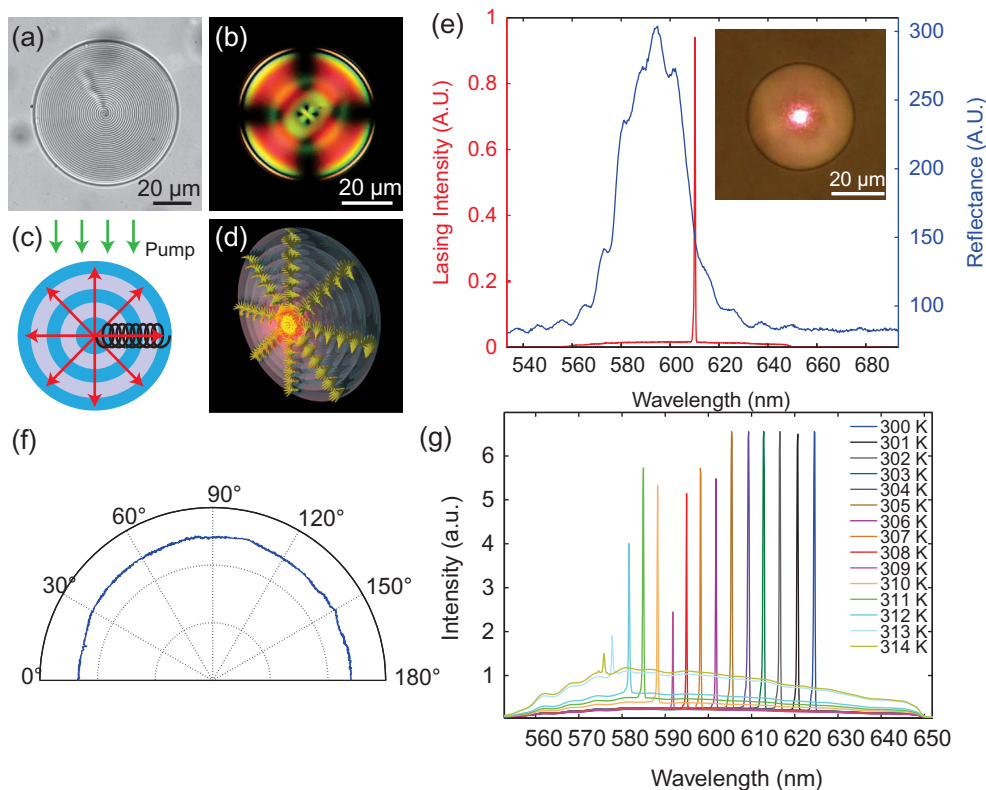


Figure 6. (a) A CLC droplet with long pitch. (b) A CLC droplet under crossed polarisers. (c) Illustration of CLC lasing mechanism in a droplet and (d) 3D rendering of the cholesteric structure. (e) Lasing spectrum (red) and reflectance of a thin layer of same CLC (blue) (inset). Image of a lasing droplet with a bright spot in the centre. (f) Angular dependence of lasing intensity. (g) Lasing spectrum at different temperatures.

polarisation are all comparable with a planar CLC laser made of the same mixture and thickness equivalent to the diameter of the droplet.

By measuring the laser output as a function of angle, we have found that the emission from the droplet is very uniform in all directions (Figure 6(f)), as well the lasing wavelength is nearly constant for different directions. This is expected, since the CLC droplets are almost spherically symmetric. Due to omnidirectional emission, the CLC droplet lasers are also referred to as 3D lasers [50]. The lasing was not specifically measured in the direction of the defect line. It would be to expect that there is no lasing emission in that direction.

3.2. Temperature tunability

CLC lasers are known to be highly tunable [53,54] by various means such as position dependent pitch, temperature, light and electric field. In some cases, emission across the entire visible spectrum was achieved from a single device. Here, the tuning of droplet CLC laser was carried out by changing the temperature. The lasing wavelength was tuned by almost 50 nm when changing the temperature by

just 14°C (Figure 6(g)). The spectral shift was almost linear with temperature, continuous and completely reversible. On the contrary, in planar CLC lasers the tunability by temperature is in most cases non-continuous, containing discrete steps in the lasing wavelength [55]. Because of planar alignment of the two confining surfaces, there is a one-half-integer number of turns in the LC layer. Therefore, the pitch changes in steps with temperature. In CLC droplets, the anchoring at the surface of the droplet is planar degenerate, which enables continuous rotation of the director at the surface.

Temperature tunability can also be a drawback if the lasers are intended to be used as light sources with fixed wavelength. This can be partially solved by using a LC with smaller temperature pitch length dependence, or by using a polymerisable CLC [56].

4. Combination of WGMs and Bragg modes

4.1. Simultaneous lasing of WGMs and Bragg modes

WGM lasing was demonstrated in nematic droplets, but droplets of cholesteric liquid crystal can also be

used for this purpose as far as the refractive index contrast and droplet size are large enough. Therefore, both WGM and Bragg lasing can occur simultaneously (Figure 7(a)). The two lasing mechanisms do not compete greatly for the available gain, since WGMs are located near the surface, while Bragg lasing has the highest intensity at the droplet centre, enabling efficient lasing of both. For the Bragg lasers in the previous section, a low refractive index LC ($n_e = 1.53$, $n_o = 1.46$) and a high refractive index external medium (glycerol, $n = 1.47$) were used to avoid WGM lasing. By using higher refractive index LC ($n_e = 1.77$, $n_o = 1.51$), both lasing mechanisms can be observed (Figure 7(b)). The WGMs are visible as a ring on the surface of the droplet and the Bragg lasing is coming from the centre of the droplet. In the spectrum, several peaks correspond to WGMs and a single peak at 610 nm corresponds to Bragg lasing. Thresholds for both Bragg and WGM lasing are dependent on droplet size and are lower in bigger droplets because of higher Q-factors (Figure 7(c)). The threshold for WGMs decreases faster with increasing droplet diameter than for Bragg lasing.

The droplets below 25 μm have lower threshold for Bragg lasing, whereas above 25 μm the threshold is lower for WGMs. The smallest droplet diameter for Bragg lasing is 15 μm and for WGM lasing is 19 μm . Therefore, by changing the droplet size, the relative lasing of the two mechanisms can be controlled. Instead of using a small refractive index contrast to inhibit WGM lasing, scattering particles could be absorbed to the surface. While WGMs are very sensitive to the surface, Bragg modes are not. On the contrary, if wanting to inhibit Bragg lasing, temperature tuning can be used to push the bandage out of the gain region or by using an electric field to unwind the helix.

4.2. Ring modes lasing

In cholesteric droplets, we can achieve lasing of higher Bragg modes that have also angular momentum. By using lower concentration of chiral dopant, the PBG can be pushed to the infrared part of the spectrum, so that it is out of the gain region of the dye and the droplet does not lase any more. This is true just for

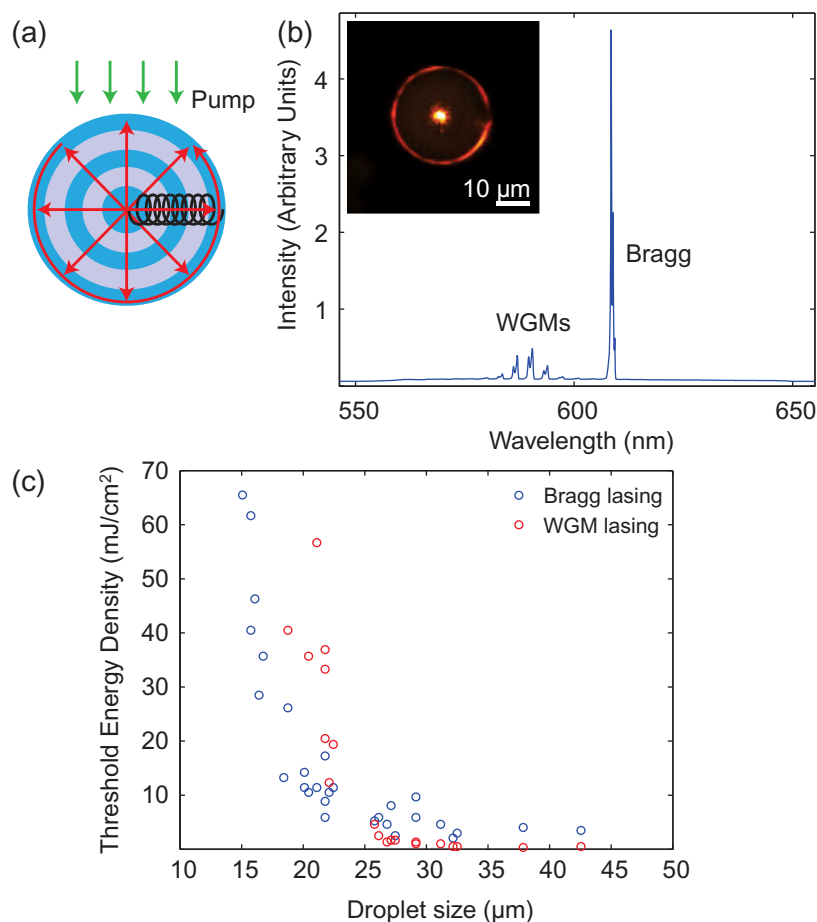


Figure 7. (Colour online) (a) Illustration of the principle of simultaneous lasing of WGMs and Bragg modes. (b) Experimental demonstration of simultaneous lasing. (c) Laser thresholds as a function of droplet size for both WGMs and Bragg lasing.

light with the incidence along the helical axis. Following the Bragg's law, at smaller angles, light with shorter wavelengths is reflected from the periodic structure. In the droplet, this means that the red fluorescent light from the dye is not any more reflected in radial direction, but instead reflects multiple times from the cholesteric layers at a smaller angle and so circulates in the droplet (Figure 8(a)). This is similar to WGMs, where the light is multiply reflected from the surface and circulates around the droplet. The difference in cholesteric droplet is that the light is not reflected because of total internal reflection, but because of Bragg structure. The light also does not circulate close to the surface, but in the interior of the droplet. A dye-doped CLC mixture with the centre of the photonic bandgap positioned at 770 nm was used. When a droplet was pumped by a pulsed laser, a ring of light was clearly visible in the interior of the droplet (Figure 8(b)). In the spectrum, several equally spaced laser lines were observed. If using even longer pitch, the ring of light becomes larger also requiring the droplet to be larger in order to support these modes. With longer pitch also, the number of modes increases.

5. Conclusions and future prospects

As demonstrated here, liquid crystal droplets can support a variety of optical modes and can be used as optical cavities and lasers. The structures in the droplets are self-assembled because of elastic forces in LCs, which is a great advantage over solid-state optical components, since no complicated fabrication methods are necessary. The second advantage is large tunability and sensitivity to external stimuli.

In this work, droplets were made by mechanical mixing which led to very polydispersed droplets. The

lasing wavelength of CLC droplets is greatly independent on the droplet size, but WGMs are highly dependent on size. Microfluidics have been employed before to produce monodispersed LC droplets [57–59] or shells [60] and the same method could also be employed for all LC droplets used here. Both WGM and Bragg lasing are not limited by spherical droplets. For example, WGMs were demonstrated in a variety of geometries, including toroids, cylinders and bottle cavities. LCs have been also shaped in different geometries such as shells [14,61], tactoids [9], rods [62,63] and fibres [64]. Lasing and light waveguiding has been demonstrated smectic self-formed fibres [31]. Instead of droplets entirely filled with LC, also shells of LC [14] could have interesting applications as optical cavities. WGMs are confined close to the surface, so they are ideal to study thin LC shells as well the thin shells enable faster tunability and better sensing. CLC shells have been used to modify the emission spectrum of a material embedded in the droplet [65] as well lasing has been demonstrated within them [60].

Tuning of CLC has been here achieved only by changing the temperature, however, a more convenient way is to use electric field. For example, tuning up to 20 nm has been achieved by applying 0.175 V/ μm electric field to CLC droplets [66]. Phototuning of lasing in CLC droplets has been demonstrated by including a chiral molecular switch which undergoes photoisomerisation when illuminated [60,67]. Ultrafast all-optical tuning can be achieved by using a femtosecond laser via a coherently excited optical Kerr effect [68] or via stimulated emission depletion [69]. Another way of tuning is by using mechanical deformation of LC droplets by stretching the polymer matrix [32,70]. Optomechanic tunable cavities could be made by using LC elastomer particles, which change shape when

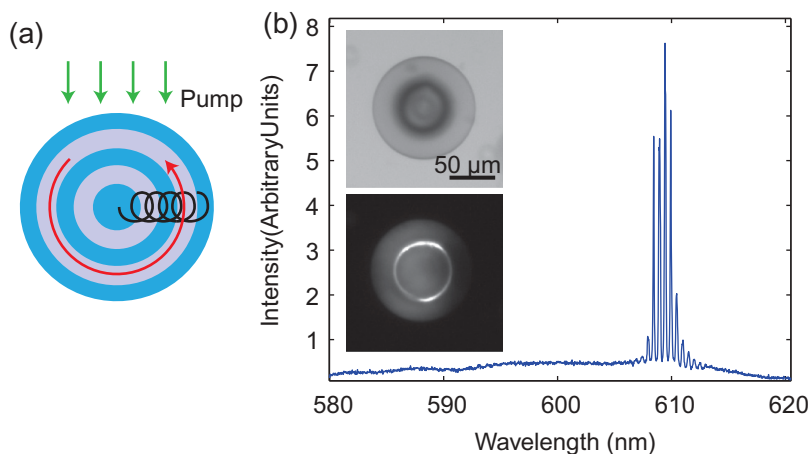


Figure 8. (Colour online) (a) Illustration of principle of ring lasing. (b) Spectrum of ring lasing, a bright-field image of a CLC droplet (top inset) and lasing (bottom inset).

illuminated [62,63]. Mechanic tuning by using flow can be even faster than electric tuning, achieving submilli-second response [71].

By polymerising the liquid crystal itself, a more mechanically stable microlaser can be made useful, for example, in biological imaging. After polymerisation, the lasers cannot be tuned any more and are insensitive to temperature changes. Before the polymerisation, they can be tuned by temperature to a particular frequency and then polymerised. Polymerised CLC droplet lasers have been already demonstrated and show good stability and lasing [56]. In a similar fashion also, WGM lasers could be polymerised.

In all the experiments in this work, the excitation and collection of light was done in far field by using a microscope. In order to integrate LC cavities to more complex optical system, a different light delivery approach should be employed. For example, evanescent field coupling of WGMs in a nematic droplet with a planar waveguide has been demonstrated [20]. Coupling the resonators with waveguides could lead to efficient extraction of light from cavities, as well as a potential to use them as filters and routers. Further, Bragg lasers could be interfaced with an end of an optical fibre. The fibre can be brought close to the surface of the droplet or even inserted into the droplet towards its centre, where there is the highest laser intensity. For example, structures of CLC droplets pierced by cellulose fibres have been studied before [72], but optical properties have not been characterised.

Here, we have only discussed optical modes in LC droplets in an isotropic fluid or solid. However, similarly also optical modes in colloids embedded in LC could be used. That is an inverted system to the LC droplets. A wide variety of very complex self-assembled colloidal structures exist in this systems, which could be used for this purpose [1–5]. Assemblies of colloids could be used as tunable self-assembled arrays of cavities such as coupled resonator optical waveguides (CROWs) [73]. Further, colloidal optical cavities could be also optically coupled to optical fibres to make optical circuits held together by elastic forces in LC [74,75].

CLC droplets are not useful only as lasers, but also as omnidirectional selective reflection elements [76–78]. Because of spherical symmetry the Bragg reflection is the same in all directions in contrast to planar CLC layers. This can lead to interesting reflection patterns [77]. The interaction of light with cholesteric particles creates a variety of chirality-induced optical forces and torques in a laser trap [79–81].

LCs are already widely applied to biomedical applications [82]. LC droplet based light sources can be

further applied to biomedical imaging, therapy and diagnosis [21,83]. WGMs in LC droplets were used only for sensing of a simple surfactant. Further investigations are required on more sophisticated systems to increase the specificity of the chemical sensing. For example, by using WGM detection of structural changes in droplets that already have extremely low detection limit for endotoxins [39] could be decreased even further. CLC hemispherical lasers have been also used as a gas sensors [84].

A number of applications of the LC cavities is anticipated such as holography, telecommunications, optical computing, imaging, ultrasensitive biosensing, temperature and displacement measurements and even as a material for paints [85,86] or light sources that emit coherent light in all directions.

Acknowledgments

I would like to thank I. Muševič, M. Ravnik and S. Pajk for their valuable contribution to this work.

Disclosure statement

No potential conflict of interest was reported by the author.

Funding

The work was supported by Marie Curie International Outgoing Fellowship Number 627274 within the 7th European Community Framework Programme and by the Slovenian Research Agency under the contracts P1-0099, PR-01557, J1-9728 and J1-3612; Directorate-General for Research and Innovation: [Grant Number 627274]; Slovenian Research Agency: [Grant Number P1-0099, PR-01557, J1-9728, J1-3612].

ORCID

Matjaž Humar  <http://orcid.org/0000-0003-3338-6723>

References

1. Muševič I, Škarabot M, Tkalec U, et al. Two-dimensional nematic colloidal crystals self-assembled by topological defects. *Science. American Association for the Advancement of Science*; 2006;313:954–958. doi:10.1126/science.1129660.
2. Smalyukh II, Lansac Y, Clark NA, et al. Three-dimensional structure and multistable optical switching of triple-twisted particle-like excitations in anisotropic fluids. *Nat Mater* [Internet]. Nature Publishing Group; 2010 Feb;9:139–145. 10.1038/nmat2592.
3. Poulin P, Stark H, Lubensky TC, et al. Novel colloidal interactions in anisotropic fluids. *Science. American Association for the Advancement of Science*; 1997;275:1770–1773. doi:10.1126/science.275.5307.1770.

4. Tkalec U, Ravnik M, Čopar S, et al. Reconfigurable knots and links in chiral nematic colloids. *Science* [Internet]. American Association for the Advancement of Science; 2011;333:62–65. doi:10.1126/science.1205705
5. Ravnik M, Škarabot M, Žumer S, et al. Entangled nematic colloidal dimers and wires. *Phys Rev Lett*. APS; 2007;99:247801. doi:10.1103/PhysRevLett.99.247801.
6. Humar M, Škarabot M, Ravnik M, et al. Electrically tunable diffraction of light from 2D nematic colloidal crystals. *Eur Phys J E*. Springer-Verlag; 2008;27:73–79. doi:10.1140/epje/i2008-10353-0.
7. Nych A, Ognysta U, Škarabot M, et al. Assembly and control of 3D nematic dipolar colloidal crystals. *Nat Commun*. Nature Publishing Group; 2013;4:1489. doi:10.1038/ncomms2486.
8. Coles H, Morris S. Liquid-crystal lasers. *Nat Photonics* [Internet]. Nature Publishing Group; 2010;4:676–685. <http://www.nature.com/doi/10.1038/nphoton.2010.184>
9. Drzaic PS. *Liquid crystal dispersions*. Singapore: World Scientific; 1995.
10. Doane JW, Vaz NA, B-G W, et al. Field controlled light scattering from nematic microdroplets. *Appl Phys Lett*. AIP Publishing; 1986;48:269–271. doi:10.1063/1.96577.
11. Hands PJW, Gardiner DJ, Morris SM, et al. Band-edge and random lasing in paintable liquid crystal emulsions. *Appl Phys Lett*. 2011;98:3–5. doi:10.1063/1.3574915.
12. Lee C-R, Lin J-D, Huang B-Y, et al. All-optically controllable random laser based on a dye-doped liquid crystal added with a photoisomerizable dye. *Opt Express*. Optical Society of America; 2010;18:25896–25905. doi:10.1364/OE.18.025896.
13. Nagai Y, Fujimura R, Kajikawa K. Coherent random laser fluid of nematic liquid crystal emulsions. *Jpn J Appl Phys* [Internet]. 2014;53:01AE05. doi:10.7567/JJAP.53.01AE05
14. Lopez-Leon T, Fernandez-Nieves A. Drops and shells of liquid crystal. *Colloid Polym Sci*. Springer; 2011;289:345–359. doi:10.1007/s00396-010-2367-7.
15. Seč D, Čopar S, Žumer S. Topological zoo of free-standing knots in confined chiral nematic fluids. *Nat Commun*. 2014;5:3057. doi:10.1038/ncomms4057.
16. Gorodetsky ML, Fomin AE. Geometrical theory of whispering-gallery modes. *Sel Top Quantum Electron*. IEEE J. 2006;12:33–39. doi:10.1109/JSTQE.2005.862954.
17. Novotny L, Hecht B. *Principles of nano-optics*. Cambridge: Cambridge University Press; 2012.
18. De Gennes PG, Prost J. *The physics of liquid crystals*. Oxford: Clarendon Press; 1993.
19. Vahala KJ. Optical microcavities. *Nature*. 2003;424:839–846. doi:10.1038/nature01939.
20. Jampani VSR, Humar M, Mušević I. Resonant transport of light from planar polymer waveguide into liquid-crystal microcavity. *Opt Express*. Optical Society of America; 2013;21:20506–20516. doi:10.1364/OE.21.020506.
21. Humar M, Hyun Yun S. Intracellular microlasers. *Nat Photonics* [Internet]. 2015;9:572–576. Available from: <http://www.nature.com/doi/10.1038/nphoton.2015.129>
22. Humar M, Ravnik M, Pajk S, et al. Electrically tunable liquid crystal optical microresonators. *Nat Photonics*. 2009;595–600. doi:10.1038/nphoton.2009.170.
23. Humar M, Mušević I. Surfactant sensing based on whispering-gallery-mode lasing in liquid-crystal microdroplets. *Opt Express*. Optical Society of America; 2011;19:19836–19844. doi:10.1364/OE.19.019836.
24. Wang T-J, Chu C-H, Lin C-Y. Electro-optically tunable microring resonators on lithium niobate. *Opt Lett*. 2007;32:2777–2779. doi:10.1364/OL.32.002777.
25. Mušević I, Škarabot M, Humar M. Direct and inverted nematic dispersions for soft matter photonics. *J Phys Condens Matter*. 2011;23:284112. doi:10.1088/0953-8984/23/28/284112.
26. Maune B, Lawson R, Gunn G, et al. Electrically tunable ring resonators incorporating nematic liquid crystals as cladding layers. *Appl Phys Lett*. 2003;83:4689–4691. doi:10.1063/1.1630370.
27. Bondar VG, Lavrentovich OD, Pergamenschik VM. Threshold of structural hedgehog-ring transition in drops of a nematic in an alternating electric field. *Sov Phys. JETP*. 1992;74:60–67.
28. Piegdon KA, Matthias H, Meier C, et al. Tunable optical properties of photonic crystals and semiconductor microdisks using liquid crystals. *Proc SPIE*. 2007;1:1–9.
29. Kiraz A, Karadağ Y, Coskun AF. Spectral tuning of liquid microdroplets standing on a superhydrophobic surface using electrowetting. *Appl Phys Lett*. 2008;92:8–10. doi:10.1063/1.2927373.
30. Kumar TA, Mohiddon MA, Dutta N, et al. Detection of phase transitions from the study of whispering gallery mode resonance in liquid crystal droplets. *Appl Phys Lett*. AIP Publishing; 2015;106:51101. doi:10.1063/1.4906615.
31. Peddireddy K, Jampani VSR, Thutupalli S, et al. Lasing and waveguiding in smectic A liquid crystal optical fibers. *Opt Express* [Internet]. 2013;21:30233–30242. doi:10.1364/OE.21.030233
32. Mušević I, Humar M. Tunable liquid crystal optical microcavities. *Spie Opto*. 2011;7955:795509.
33. Dong CH, He L, Xiao YF, et al. Fabrication of high-Q polydimethylsiloxane optical microspheres for thermal sensing. *Appl Phys Lett*. 2009;94:3–5. doi:10.1063/1.3152791.
34. Ma Q, Rossmann T, Guo Z. Whispering-gallery mode silica microsensors for cryogenic to room temperature measurement. *Meas Sci Technol*. IOP Publishing; 2010;21:25310. doi:10.1088/0957-0233/21/2/025310.
35. Vollmer F, Arnold S. Whispering-gallery-mode biosensing: label-free detection down to single molecules. *Nat Methods*. 2008;5:591–596. doi:10.1038/nmeth.1221.
36. Armani AM, Kulkarni RP, Fraser SE, et al. Label-free, single-molecule detection with optical microcavities. *Science* [Internet]. 2007;317:783–787. doi:10.1126/science.1145002
37. Brake JM, Daschner MK, Luk -Y-Y, et al. Biomolecular interactions at phospholipid-decorated surfaces of liquid crystals. *Science*. American Association for the Advancement of Science; 2003;302:2094–2097. doi:10.1126/science.1091749.
38. Dubtsov AV, Pasechnik SV, Shmeliova DV, et al. Light and phospholipid driven structural transitions in

- nematic microdroplets. *Appl Phys Lett*. AIP Publishing; 2014;105:151606. doi:10.1063/1.4898335.
39. Lin I, Miller DS, Bertics PJ, et al. Endotoxin-induced structural transformations in liquid crystalline droplets. *Science* [Internet]. 2011;332:1297–1300. doi:10.1126/science.1195639
40. Lee K, Gupta KC, Park S-Y, et al. Anti-IgG-anchored liquid crystal microdroplets for label free detection of IgG. *J Mater Chem B*. Royal Society of Chemistry; 2016;4:704–715. doi:10.1039/C5TB02131F.
41. Sivakumar S, Wark KL, Gupta JK, et al. Liquid crystal emulsions as the basis of biological sensors for the optical detection of bacteria and viruses. *Adv Funct Mater*. 2009;19:2260–2265. doi:10.1002/adfm.v19:14.
42. Yoon SH, Gupta KC, Borah JS, et al. Folate ligand anchored liquid crystal microdroplets emulsion for in vitro detection of KB cancer cells. *Langmuir*. ACS Publications; 2014;30:10668–10677. doi:10.1021/la502032k.
43. Takezoe H. Liquid crystal lasers. In: *Liquid crystals beyond displays: chemistry, physics, and applications*. Hoboken, NJ: John Wiley & Sons; 2012.
44. Blanco A, Chomski E, Grabtchak S, et al. Large-scale synthesis of a silicon photonic crystal with a complete three-dimensional bandgap near 1.5 micrometres. *Nat* [Internet]. 2000 May;405:437–440. doi:10.1038/35013024.
45. Tandraechanurat A, Ishida S, Guimard D, et al. Lasing oscillation in a three-dimensional photonic crystal nanocavity with a complete bandgap. *Nat Photonics*. Nature Publishing Group; 2011;5:91–94. doi:10.1038/nphoton.2010.286.
46. Cao W, Muñoz A, Palfy-Muhoray P, et al. Lasing in a three-dimensional photonic crystal of the liquid crystal blue phase II. *Nat Mater*. 2002;1:111–113. doi:10.1038/nmat727.
47. Scheuer J, Green WMJ, DeRose G, et al. Low-threshold two-dimensional annular Bragg lasers. *Opt Lett*. 2004;29:2641–2643. doi:10.1364/OL.29.002641.
48. Gourevich I, Field LM, Wei Z, et al. Polymer multilayer particles: a route to spherical dielectric resonators. *Macromolecules*. 2006;39:1449–1454. doi:10.1021/ma052167o.
49. Zhang K, Gao L, Chen Y, et al. Onion-like microspheres with tricomponent from gelable triblock copolymers. *J Colloid Interface Sci* [Internet]. Elsevier Inc.; 2010; 346:48–53. doi:10.1016/j.jcis.2010.02.039.
50. Humar M, Mušević I. 3D microlasers from self-assembled cholesteric liquid-crystal microdroplets. *Opt Express*. 2010;18:26995–27003. doi:10.1364/OE.18.026995.
51. Bezic J, Žumer S. Structures of the cholesteric liquid-crystal droplets with parallel surface anchoring. *Liq Cryst*. 1992;11:593–619. doi:10.1080/02678299208029013.
52. Seč D, Porenta T, Ravnik M, et al. Geometrical frustration of chiral ordering in cholesteric droplets. *Soft Matter*. Royal Society of Chemistry; 2012;8:11982–11988. doi:10.1039/c2sm27048j.
53. Sonoyama K, Takanishi Y, Ishikawa K, et al. Position-sensitive cholesteric liquid crystal dye laser covering a full visible range. *Japanese J Appl Physics, Part 2 Lett*. 2007;46:874–876. doi:10.1143/JJAP.46.L874.
54. Manabe T, Sonoyama K, Takanishi Y, et al. Toward practical application of cholesteric liquid crystals to tunable lasers. *J Mater Chem* [Internet]. 2008;18:3040–3043. doi:10.1039/B802461H.
55. Morris SM, Ford AD, Coles HJ. Removing the discontinuous shifts in emission wavelength of a chiral nematic liquid crystal laser. *J Appl Phys* [Internet]. 2009;106. Available from: <http://scitation.aip.org/content/aip/journal/jap/106/2/10.1063/1.3177251>
56. Cipparrone G, Mazzulla A, Pane A, et al. Chiral self-assembled solid microspheres: a novel multifunctional microphotonic device. *Adv Mater*. 2011;23:5773–5778. doi:10.1002/adma.v23.48.
57. Hamlington BD, Steinhaus B, Feng JJ, et al. Liquid crystal droplet production in a microfluidic device. *Liq Cryst*. 2007;34:861–870. doi:10.1080/02678290601171485.
58. Belloul M, Bartolo J-F, Ziraoui B, et al. High-throughput formation and control of monodisperse liquid crystals droplets driven by an alternating current electric field in a microfluidic device. *Appl Phys Lett*. AIP Publishing; 2013;103:33112. doi:10.1063/1.4813880.
59. Priest C, Quinn A, Postma A, et al. Microfluidic polymer multilayer adsorption on liquid crystal droplets for microcapsule synthesis. *Lab Chip*. Royal Society of Chemistry; 2008;8:2182–2187. doi:10.1039/b808826h.
60. Chen L, Li Y, Fan J, et al. photoresponsive monodisperse cholesteric liquid crystalline microshells for tunable omnidirectional lasing enabled by a visible light-driven chiral molecular switch. *Adv Opt Mater*. 2014;2:845–848. doi:10.1002/adom.201400166.
61. Fernández-Nieves A, Vitelli V, Utada AS, et al. Novel defect structures in nematic liquid crystal shells. *Phys Rev Lett*. APS; 2007;99:157801. doi:10.1103/PhysRevLett.99.157801.
62. Ohm C, Serra C, Zentel R. A continuous flow synthesis of micrometer-sized actuators from liquid crystalline elastomers. *Adv Mater*. Wiley Online Library; 2009;21:4859–4862. doi:10.1002/adma.200901522.
63. Sun Y, Evans JS, Lee T, et al. Optical manipulation of shape-morphing elastomeric liquid crystal microparticles doped with gold nanocrystals. *Appl Phys Lett*. AIP Publishing; 2012;100:241901. doi:10.1063/1.4729143.
64. Peddireddy K, Kumar P, Thutupalli S, et al. Myelin structures formed by thermotropic smectic liquid crystals. *Langmuir* [Internet]. 2013;29:15682–15688. doi:10.1021/la4038588.
65. Iwai Y, Kaji H, Uchida Y, et al. Chemiluminescence emission in cholesteric liquid crystalline core-shell microcapsules. *J Mater Chem C* [Internet]. The Royal Society of Chemistry; 2014; 2:4904–4908. doi:10.1039/C4TC00699B.
66. Mušević I, Peng H, Nikkhou M, et al. Self-assembled liquid-crystal microlasers, microresonators, and microfibres. *Spie Lase*. 2014;8960:896016.
67. Lin J-D, Hsieh M-H, Wei G-J, et al. Optically tunable/switchable omnidirectionally spherical microlaser based on a dye-doped cholesteric liquid crystal microdroplet with an azo-chiral dopant. *Opt Express* [Internet]. OSA; 2013 Jul;21:15765–15776. doi:10.1364/OE.21.015765.
68. Cattaneo L, Savoini M, Mušević I, et al. Ultrafast all-optical response of a nematic liquid crystal. *Opt Express* [Internet]. OSA; 2015 Jun;23:14010–14017. doi:10.1364/OE.23.014010.

69. Vitek M, Muševič I. Nanosecond control and optical pulse shaping by stimulated emission depletion in a liquid crystal. *Opt Express* [Internet]. OSA; 2015 Jun;23:16921–16932. doi:10.1364/OE.23.016921.
70. Shibaev PV, Crooker B, Manevich M, et al. Mechanically tunable microlasers based on highly viscous chiral liquid crystals. *Appl Phys Lett* [Internet]. 2011;99. Available from: <http://scitation.aip.org/content/aip/journal/apl/99/23/10.1063/1.3665943>
71. Cuennet JG, Vasdekis AE, De Sio L, et al. Optofluidic modulator based on peristaltic nematogen microflows. *Nat Photonics*. Nature Publishing Group; 2011;5:234–238. doi:10.1038/nphoton.2011.18.
72. Geng Y, Sec D, Almeida PL, et al. Liquid crystal necklaces: cholesteric drops threaded by thin cellulose fibres. *Soft Matter* [Internet]. The Royal Society of Chemistry; 2013; 9:7928–7933. doi:10.1039/C3SM50900A.
73. Poon JKS, Zhu L, DeRose GA, et al. Polymer microring coupled-resonator optical waveguides. *Light Technol J. IEEE*; 2006;24:1843–1849. doi:10.1109/JLT.2006.870971.
74. Nikkhou M, Škarabot M, Čopar S, et al. Light-controlled topological charge in a nematic liquid crystal. *Nat Phys*. Nature Publishing Group; 2015;11:183–187. doi:10.1038/nphys3194.
75. Nikkhou M, Škarabot M, Muševič I. Topological binding and elastic interactions of microspheres and fibres in a nematic liquid crystal. *Eur Phys J E*. Springer; 2015;38:1–15. doi:10.1140/epje/i2015-15023-6.
76. Beltran-Gracia E, Parri OL. A new twist on cholesteric films by using reactive mesogen particles. *J Mater Chem C*. Royal Society of Chemistry; 2015;3:11335–11340. doi:10.1039/C5TC02920A.
77. Noh J, Liang H-L, Drevensek-Olenik I, et al. Tuneable multicoloured patterns from photonic cross-communication between cholesteric liquid crystal droplets. *J Mater Chem C* [Internet]. The Royal Society of Chemistry; 2014; 2:806–810. doi:10.1039/C3TC32055C.
78. Fan J, Li Y, Bisoyi HK, et al. Light-directing omnidirectional circularly polarized reflection from liquid-crystal droplets. *Angew Chemie* [Internet]. WILEY-VCH Verlag; 2015; 127:2188–2192. doi:10.1002/ange.201410788.
79. Donato MG, Hernandez J, Mazzulla A, et al. Polarization-dependent optomechanics mediated by chiral microresonators. *Nat Commun*. Nature Publishing Group; 2014;5. doi:10.1038/ncomms4656.
80. Tkachenko G, Brasselet E. Helicity-dependent three-dimensional optical trapping of chiral microparticles. *Nat Commun*. Nature Publishing Group; 2014;5. doi:10.1038/ncomms5491.
81. Yang Y, Brimicombe PD, Roberts NW, et al. Continuously rotating chiral liquid crystal droplets in a linearly polarized laser trap. *Opt Express* [Internet]. OSA; 2008 May;16:6877–6882. doi:10.1364/OE.16.006877.
82. Woltman SJ, Jay GD, Crawford GP. Liquid-crystal materials find a new order in biomedical applications. *Nat Mater*. Nature Publishing Group; 2007;6:929–938. doi:10.1038/nmat2010.
83. Humar M, Kwok SJJ, Choi M, et al. Towards biomaterial-based implantable photonic devices. *Nanophotonics*. De Gruyter; 2016;5:60–80. doi:10.1515/nanoph-2016-0003.
84. Ta VD, Chen R, Nguyen DM, et al. Application of self-assembled hemispherical microlasers as gas sensors. *Appl Phys Lett* [Internet]. 2013;102. Available from: <http://scitation.aip.org/content/aip/journal/apl/102/3/10.1063/1.4788751>
85. Hands PJW, Gardiner DJ, Morris SM, et al. Band-edge and random lasing in paintable liquid crystal emulsions. *Appl Phys Lett*. AIP Publishing; 2011;98:141102. doi:10.1063/1.3574915.
86. Gardiner DJ, Morris SM, Hands PJW, et al. Paintable band-edge liquid crystal lasers. *Opt Express*. 2011;19:2432–2439.